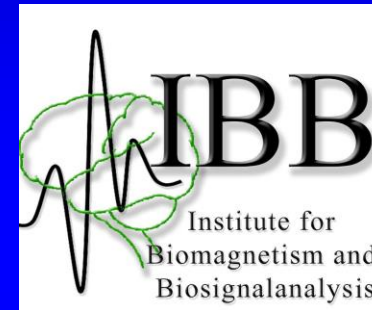


Mathematical Methods for the Registration of Medical Images, Part II

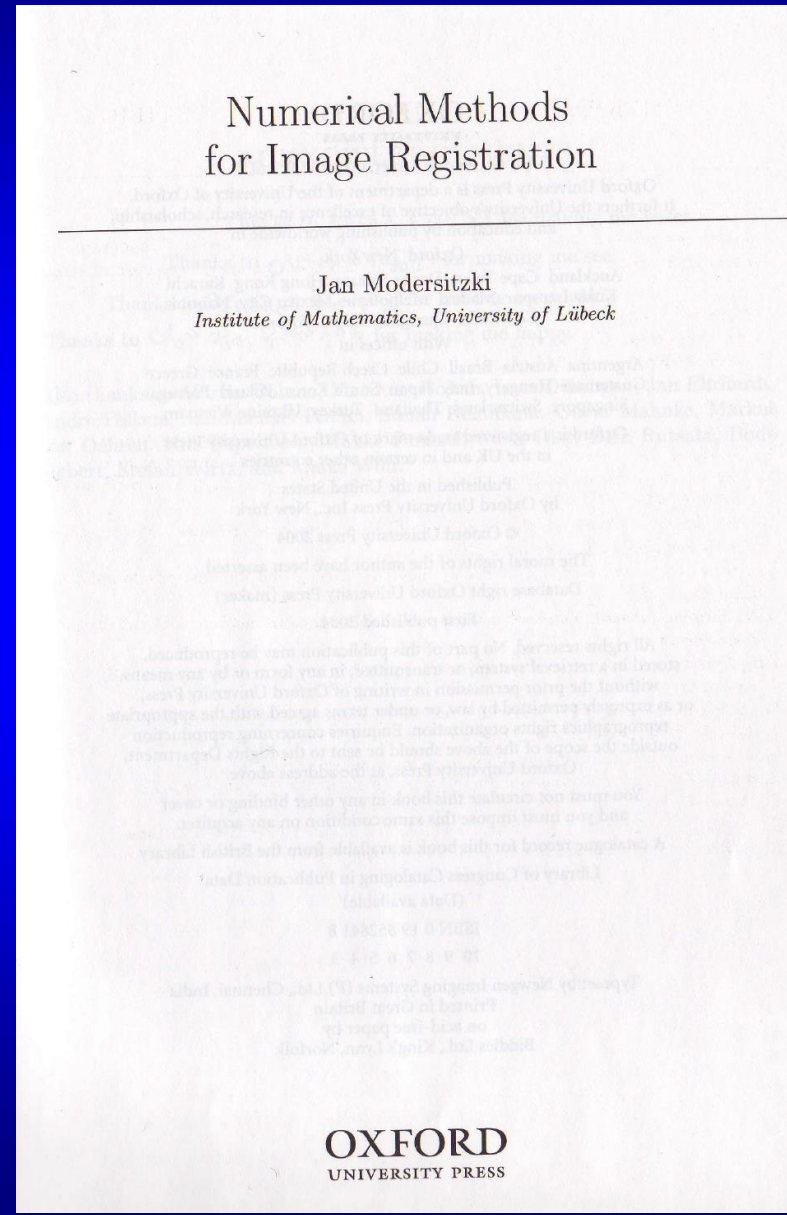
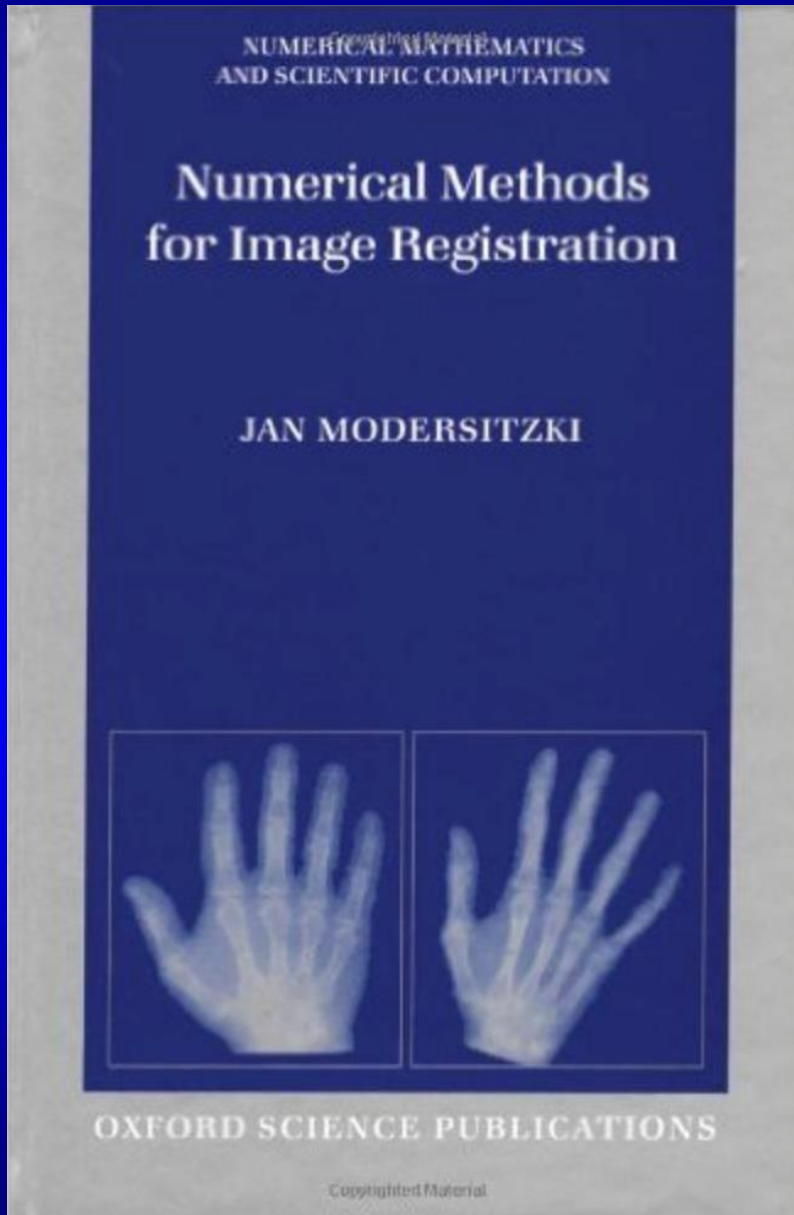


Carsten Wolters

Institut für Biomagnetismus und Biosignalanalyse, Westfälische Wilhelms-Universität Münster

Lecture, April 22, 2025

Literature



Structure

- **Parametric image registration techniques**
- **Non-parametric image registration techniques**
- **Non-parametric registration for DTI**

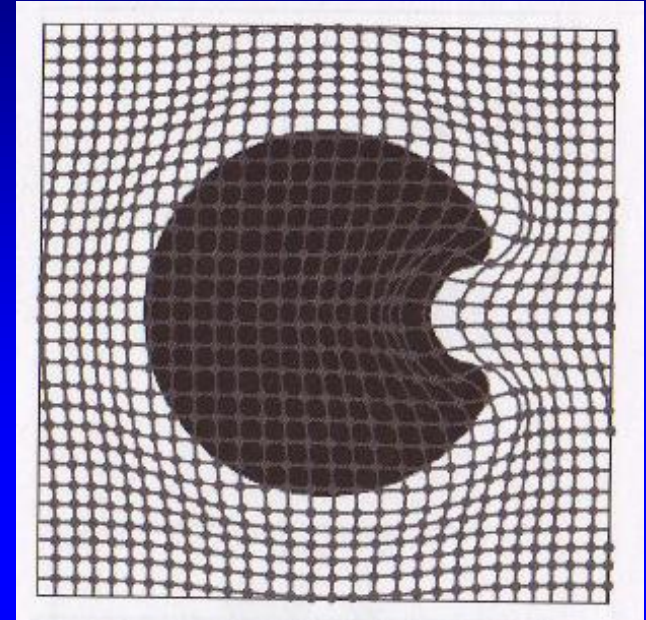
General framework

$$\varphi(x) = x - u(x)$$

$$T_u(x) := T(x - u(x)) = T(\varphi(x))$$

$$\mathcal{D}[R, T; u] := \mathcal{D}[R, T_u] \xrightarrow{u} \min$$

$$\mathcal{S}[u] = \frac{1}{2}a[u, u]$$



Problem 8.1 Given two images R , T , and a positive regularizing parameter $\alpha \in \mathbb{R}_{>0}$, find a deformation u , such that

$$\mathcal{J}[u] := \mathcal{D}[R, T; u] + \alpha\mathcal{S}[u] = \min.$$

General framework: Gateau differentiability

$$\begin{aligned} d\mathcal{S}[u; v] &= \lim_{h \rightarrow 0} \frac{1}{2h} (a[u + hv, u + hv] - a[u, u]) = a[u, v] \\ &= \int_{\mathbb{R}^d} \langle \mathcal{A}[u](x), v(x) \rangle_{\mathbb{R}^d} dx. \end{aligned} \quad (8.4)$$

General framework

Theorem 8.1 Let $d \in \mathbb{N}$ and $R, T \in \text{Img}(d)$, $T \in C^2(\mathbb{R}^d)$, $u, v : \mathbb{R}^d \rightarrow \mathbb{R}^d$, $\Omega :=]0, 1[^d$. The Gâteaux derivative of $\mathcal{D}[R, T; u]$,

$$\mathcal{D}[R, T; u] := \mathcal{D}^{\text{SSD}}[R, T_u] := \frac{1}{2} \|T_u - R\|_{L_2(\Omega)} \quad (8.10)$$

with respect to v is given by

$$d\mathcal{D}[R, T; u; v] = - \int_{\mathbb{R}^d} \langle f(x, u(x)), v(x) \rangle_{\mathbb{R}^d} dx,$$

where $f : \mathbb{R}^d \times \mathbb{R}^d \rightarrow \mathbb{R}^d$,

$$f(x, u(x)) := (R(x) - T_u(x)) \nabla T_u(x). \quad (8.11)$$

General framework

Proof We take advantage of a Taylor expansion of $T(x - u(x) - hv(x))$ with respect to h at the expanding point $x - u(x)$,

$$T(x - u(x) - hv(x)) = T_u(x) - h \langle \nabla T_u(x), v(x) \rangle_{\mathbb{R}^d} + \mathcal{O}(h^2).$$

Thus,

$$\begin{aligned} d\mathcal{D}[R, T; u; v] &= \lim_{h \rightarrow 0} \frac{1}{h} (\mathcal{D}[R, T; u + hv] - \mathcal{D}[R, T; u]) \\ &= \lim_{h \rightarrow 0} \frac{1}{2h} \int_{\Omega} (T_u(x) - h \langle \nabla T_u(x), v(x) \rangle_{\mathbb{R}^d} + \mathcal{O}(h^2) - R(x))^2 \\ &\quad - (T_u(x) - R(x))^2 dx \\ &= \int_{\Omega} \langle (R(x) - T_u(x)) \nabla T_u(x), v(x) \rangle_{\mathbb{R}^d} dx. \end{aligned}$$

□

General framework: Euler-Lagrange equations

$$\begin{aligned} d\mathcal{S}[u; v] &= \lim_{h \rightarrow 0} \frac{1}{2h} (a[u + hv, u + hv] - a[u, u]) = a[u, v] \\ &= \int_{\mathbb{R}^d} \langle \mathcal{A}[u](x), v(x) \rangle_{\mathbb{R}^d} dx, \end{aligned} \quad (8.4)$$

$$d\mathcal{D}[u; v] = \int_{\mathbb{R}^d} \langle f(x, u(x)), v(x) \rangle_{\mathbb{R}^d} dx$$

$$\mathcal{A}[u](x) - f(x, u(x)) = 0, \quad \text{for all } x \in \Omega, \quad (8.5)$$

$$\mathcal{A}[u^{(k+1)}](x) = f(x, u^{(k)}(x)), \quad x \in \Omega, \quad k \in \mathbb{N}_0. \quad (8.6)$$

General framework: Discretization

$$\partial_{x_j x_j} g(x) = \frac{g(x + h_j e_j) - 2g(x) + g(x - h_j e_j)}{h_j^2} + \mathcal{O}(h_j^2), \quad (8.12)$$

$$\begin{aligned} \partial_{x_j x_k} g(x) = & \frac{1}{4h_j h_k} (g(x + h_j e_j + h_k e_k) - g(x - h_j e_j + h_k e_k) \\ & - g(x + h_j e_j - h_k e_k) + g(x - h_j e_j - h_k e_k)) \\ & + \mathcal{O}(h_j^2 + h_k^2), \end{aligned} \quad (8.13)$$

$$A \cdot \vec{g} := (S^A * g)(\vec{X})$$

S^A denotes a convolution filter connected with the PD operator A and with a lexicographical ordering of the grid points, a linear equation system arises.

General framework: The algorithm for non-parametric registration

Algorithm 8.2 *General registration algorithm.*

Initialize $k = 0$, $\vec{X}^{(k)}$, and $\vec{U}^{(k)} = 0$.

For $k = 0, 1, 2, \dots$

 compute force $\vec{F}^{(k)} = f(\vec{X}, \vec{U}^{(k)})$;

 solve partial differential equation, $A\vec{U}^{(k+1)} = \vec{F}^{(k)}$;

 if converged, stop, end;

end.

Structure

- **Non-parametric image registration techniques**
 - Elastic registration
 - **Fluid registration**

Elastic registration using Navier-Lamé equation

$$a[u, v] := \int_{\Omega} \mu \sum_{k=1}^d \langle \nabla u_k + \partial_{x_k} u, \nabla v_k \rangle_{\mathbb{R}^d} + \lambda \operatorname{div} u \operatorname{div} v \, dx \quad (9.12)$$

$$b[v] := \int_{\Omega} \langle f, v \rangle_{\mathbb{R}^d} \, dx. \quad (9.13)$$

$$\mathcal{J}[u] := \frac{1}{2} a[u, u] + b[u], \quad (9.14)$$

Theorem 9.4 *Let \mathcal{J} be defined by eqn (9.14), a be defined by eqn (9.12), and b be defined by eqn (9.13), respectively. Moreover, let $u \in (C^2(\mathbb{R}^d))^d$. For the perturbation $v \in (C^2(\mathbb{R}^d))^d$, the Gâteaux derivative of \mathcal{J} is given by*

$$d\mathcal{J}[u; v] = \int_{\Omega} \langle f - \mu \Delta u - (\mu + \lambda) \nabla \operatorname{div} u, v \rangle_{\mathbb{R}^d} \, dx.$$

Elastic registration

Proof A computation gives

$$\begin{aligned}d\mathcal{J}[u; v] &= \lim_{h \rightarrow 0} \frac{1}{h} (\mathcal{J}[u + hv] - \mathcal{J}[u]) = a[u, v] + b[v] \\ &= \int_{\Omega} \sum_{k=1}^d \mu \langle \nabla u_k + \partial_{x_k} u, \nabla v_k \rangle_{\mathbb{R}^d} + \lambda \operatorname{div} u \operatorname{div} v + \langle f, v \rangle_{\mathbb{R}^d} dx \\ &= \int_{\partial\Omega} \mu \sum_{k=1}^d v_k \langle \nabla u_k + \partial_{x_k} u, \vec{n} \rangle_{\mathbb{R}^d} + \lambda \operatorname{div} u \langle v, \vec{n} \rangle_{\mathbb{R}^d} dx \\ &\quad + \int_{\Omega} \langle f - \mu \Delta u - (\mu + \lambda) \nabla \operatorname{div} u, v \rangle_{\mathbb{R}^d} dx,\end{aligned}$$

where \vec{n} denotes the outer normal vector on $\partial\Omega$. Exploiting the implicit boundary conditions $\operatorname{div} u = \langle \nabla u_k + \partial_{x_k} u, \vec{n} \rangle_{\mathbb{R}^d} = 0$ on $\partial\Omega$, the boundary integral vanishes, which completes the proof. \square

Elastic registration

- The arising PDE is called the Navier-Lamé equation.
- The proof of the Theorem shows that implicit boundary conditions are needed. $\operatorname{div} u = \langle \nabla u_k + \partial_{x_k} u, \vec{n} \rangle_{\mathbb{R}^d} = 0$ on $\partial\Omega$,
- In practice: Influence of boundary conditions is limited, therefore explicit periodic boundary conditions are often used, since they allow the computation of eigenfunctions and eigenvalues of the Navier-Lamé operator and thus the development of an $O(N \log N)$ direct FFT-solver of the discrete system.

$$u_1(0, x_2, x_3) = u_1(1, x_2, x_3)$$

$$u_2(x_1, 0, x_3) = u_2(x_1, 1, x_3)$$

$$u_3(x_1, x_2, 0) = u_3(x_1, x_2, 1)$$

- Elastic registration needs affine pre-registration since it penalizes linear deformations $u(x)=Cx+d$

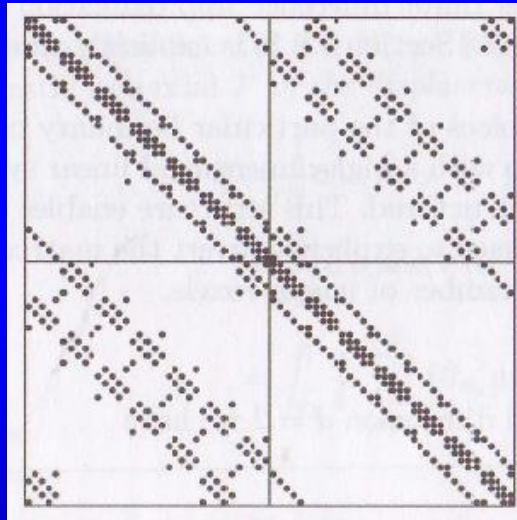
Elastic registration

$$\begin{aligned} \mathcal{A}[u] &= \mu \Delta u + (\lambda + \mu) \nabla \operatorname{div} u \\ &= \begin{pmatrix} (\lambda + 2\mu) \partial_{x_1 x_1} u_1 + \mu \partial_{x_2 x_2} u_1 + (\lambda + \mu) \partial_{x_1 x_2} u_2 \\ (\lambda + \mu) \partial_{x_1 x_2} u_1 + \mu \partial_{x_1 x_1} u_2 + (\lambda + 2\mu) \partial_{x_2 x_2} u_2 \end{pmatrix} \end{aligned}$$

$$\begin{aligned} \mathcal{A}[u](X) &= \begin{pmatrix} \mathcal{A}^{1,1}[u_1](X) + \mathcal{A}^{1,2}[u_2](X) \\ \mathcal{A}^{2,1}[u_1](X) + \mathcal{A}^{2,2}[u_2](X) \end{pmatrix} \\ &\approx \begin{pmatrix} S^{1,1} * u_1(X) + S^{1,2} * u_2(X) \\ S^{2,1} * u_1(X) + S^{2,2} * u_2(X) \end{pmatrix} \end{aligned}$$

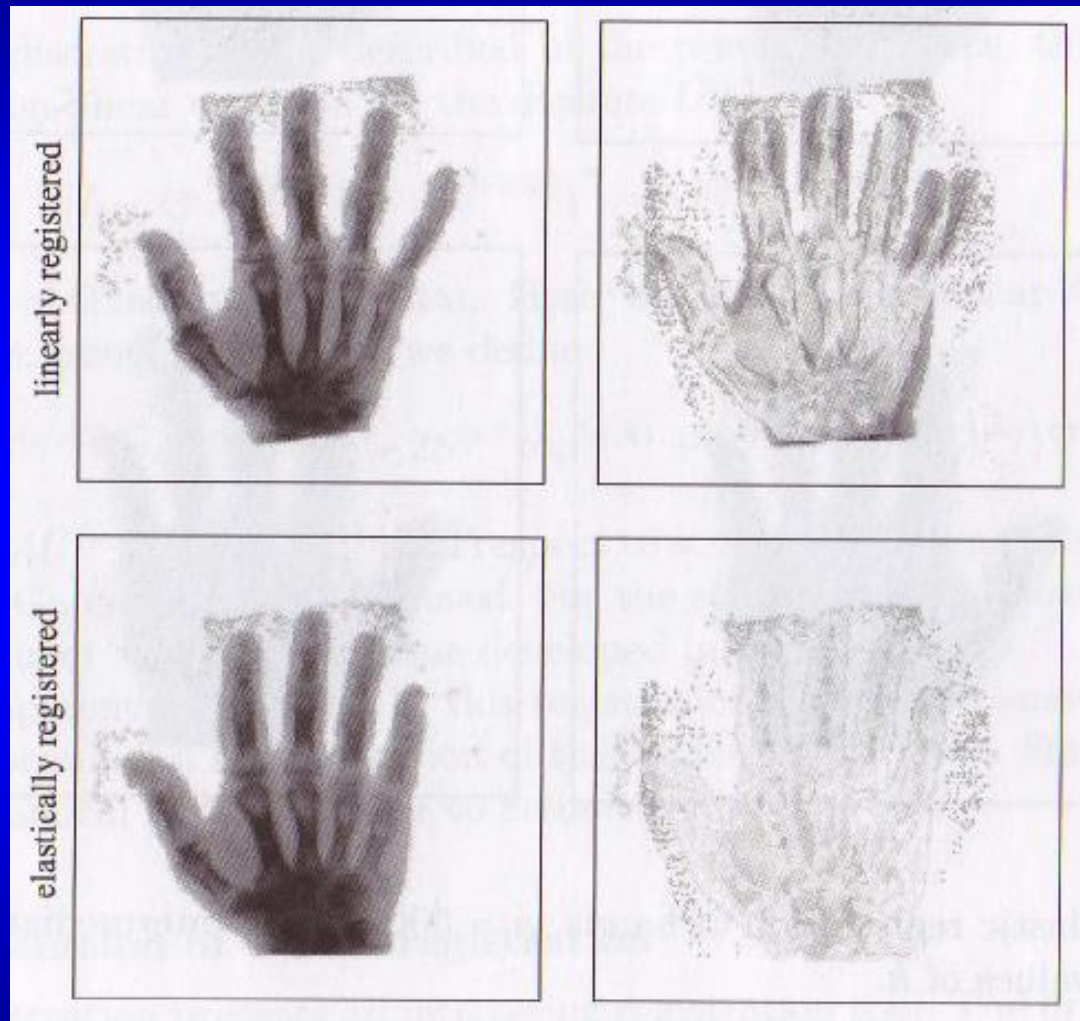
$$\mathcal{A}[u](\vec{X}) \approx \begin{pmatrix} A^{1,1} u_1(\vec{X}) + A^{1,2} u_2(\vec{X}) \\ A^{2,1} u_1(\vec{X}) + A^{2,2} u_2(\vec{X}) \end{pmatrix} =: A \vec{u}.$$

$$\begin{aligned} S^{1,1} &:= (S^{2,2})^\top = \begin{pmatrix} 0 & (\lambda + 2\mu) & 0 \\ \mu & -2(\lambda + 3\mu) & \mu \\ 0 & (\lambda + 2\mu) & 0 \end{pmatrix} \\ S^{1,2} &:= (S^{2,1})^\top := \frac{\lambda + \mu}{4} \begin{pmatrix} 1 & 0 & -1 \\ 0 & 0 & 0 \\ -1 & 0 & 1 \end{pmatrix} \end{aligned}$$



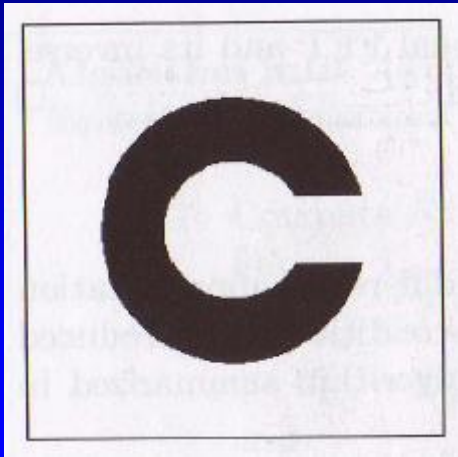
A ($n_1=5, n_2=7$) for periodic boundary conditions

Elastic registration: An example

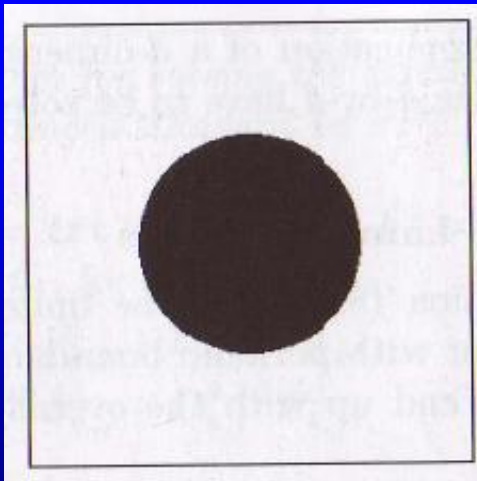


**Result for periodic boundary conditions
 $\lambda=0$, $\mu=500$**

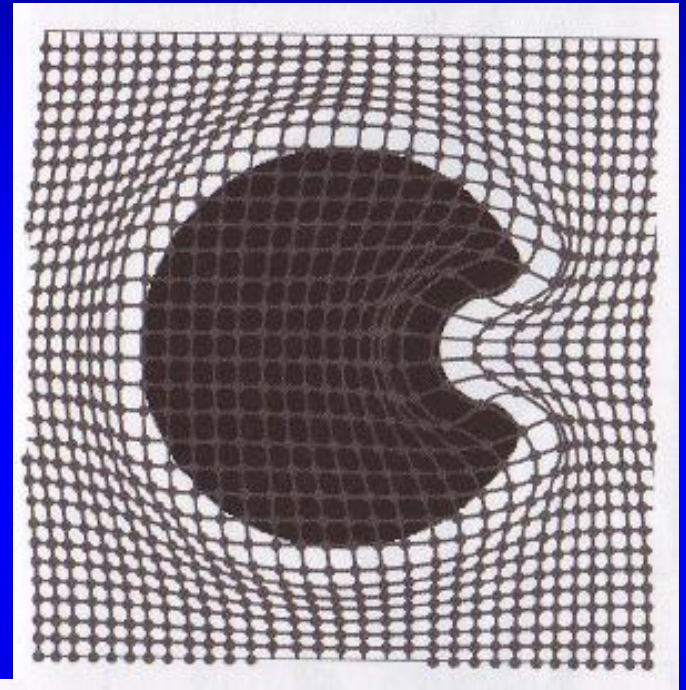
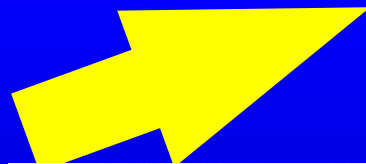
Elastic registration: An example



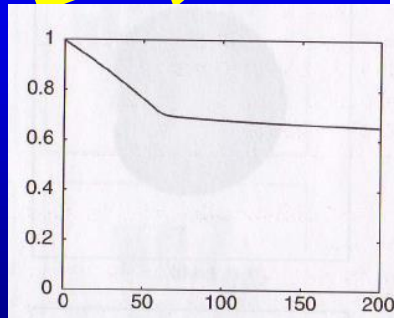
Reference image



Template image



Result for periodic
boundary conditions
 $\lambda=0$, $\mu=5000$



Structure

- **Non-parametric image registration techniques**
 - **Elastic registration**
 - Fluid registration

Fluid registration

$$\tilde{x} = \varphi(x, t) = x + u(x, t)$$

$$x = \tilde{\varphi}(\tilde{x}, t) = \tilde{x} - \tilde{u}(\tilde{x}, t),$$

Fluid registration

$$\tilde{x} = \varphi(x, t) = x + u(x, t)$$

$$x = \tilde{\varphi}(\tilde{x}, t) = \tilde{x} - \tilde{u}(\tilde{x}, t),$$

Using the initial coordinates x of the particles P as the reference coordinate system is also called the Lagrange frame, whereas tracking the particles with respect to their actual position \tilde{x} is called the Euler frame; see also Section 3.3.2 and Remark 9.2. Since the displacement and the velocity of a particle are physical properties and thus independent of the reference frame, we have

$$u(x, t) = \tilde{u}(\tilde{x}, t) \quad \text{and} \quad v(x, t) = \tilde{v}(\tilde{x}, t),$$

where the velocity of the particle P is defined as the partial time derivative of the transformation,

$$v(x, t) := \partial_t \varphi(x, t), \quad x = \varphi(P, 0).$$

Note that

$$\tilde{v}(\tilde{x}, t) = \frac{d}{dt} \tilde{u}(\tilde{x}, t) = \nabla \tilde{u}(\tilde{x}, t) \underbrace{\partial_t \tilde{x}}_{\substack{\partial_t \varphi(P, t) \\ \text{Remark 9.2}}} + \partial_t \tilde{u}(\tilde{x}, t) = \nabla \tilde{u}(\tilde{x}, t) \tilde{v}(\tilde{x}, t) + \partial_t \tilde{u}(\tilde{x}, t).$$

Fluid registration

- For Stokes fluids with very slow motion flow, we get the PDE for fluid registration:

$$\mu\Delta\tilde{v} + (\lambda + \mu)\nabla\operatorname{div}\tilde{v} = \tilde{f} \quad \tilde{v} = \partial_t\tilde{u} + \nabla\tilde{u}\tilde{v}$$

Fluid registration

- The only difference to the algorithm of elastic registration is the additional Euler step to compute the deformation from the

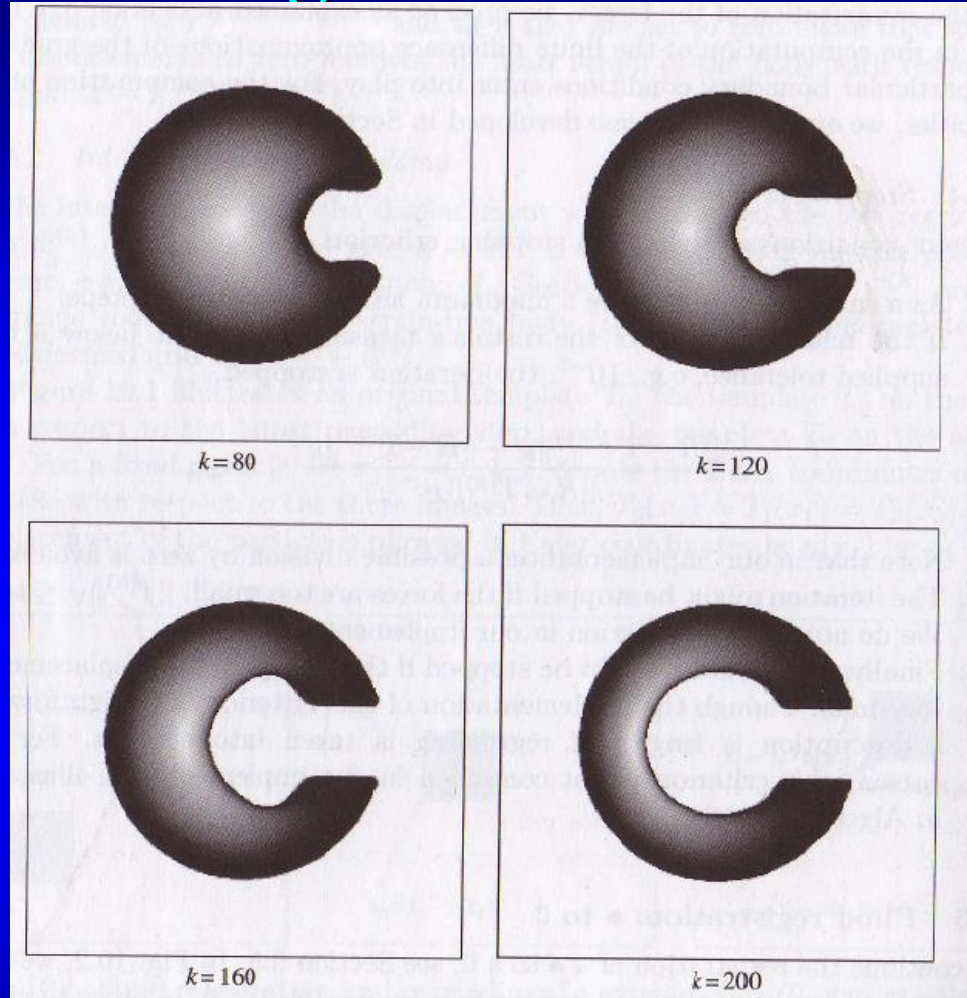
velocity following $\tilde{v} = \partial_t \tilde{u} + \nabla \tilde{u} \tilde{v}$

- The Euler step can be implemented using a centered finite difference approximation for $\nabla \tilde{u}$ and a forward FD approx. for $\partial_t \tilde{u}$

$$\hat{J}_i^{(k)} := \left(\hat{J}_{i;\ell,q}^{(k)} \right)_{\ell,q=1,\dots,d}, \quad \text{where } \hat{J}_{i;\ell,q}^{(k)} := \frac{1}{2} \left(U_{i+e_q}^{(k,\ell)} - U_{i-e_q}^{(k,\ell)} \right)$$

$$\frac{\vec{U}_i^{(k+1)} - \vec{U}_i^{(k)}}{\tau} = \left(I_d - \hat{J}_i^{(k)} \right) \vec{V}_i^{(k)}$$

Fluid registration: An example



Result for periodic boundary conditions. $\lambda=0$, $\mu=5000$.

Fluid registration provides a powerful tool since in principle, it is possible to deform any template to any reference image. However, especially this feature is certainly not appropriate for certain applications, since physically elastic objects like brains do not deform in general like honey.

Structure

- **Parametric image registration techniques**
- **Non-parametric image registration techniques**
- **Non-parametric registration for DTI**



Diffeomorphic susceptibility artifact correction of diffusion-weighted magnetic resonance images

L Ruthotto^{1,2,3}, H Kugel⁴, J Olesch^{1,5,6}, B Fischer^{1,5}, J Modersitzki¹,
M Burger³ and C H Wolters²

¹ Institute of Mathematics and Image Computing, University of Lübeck, Germany

² Institute for Biomagnetism and Biosignalanalysis, University of Münster, Germany

³ Institute for Computational and Applied Mathematics, University of Münster, Germany

⁴ Department of Clinical Radiology, University of Münster, Germany

⁵ Fraunhofer MEVIS, Project Group Image Registration, Lübeck, Germany

⁶ Graduate School for Computing in Medicine and Life Sciences, University of Lübeck, Germany

E-mail: lars.ruthotto@mic.uni-luebeck.de

Received 14 February 2012, in final form 18 June 2012

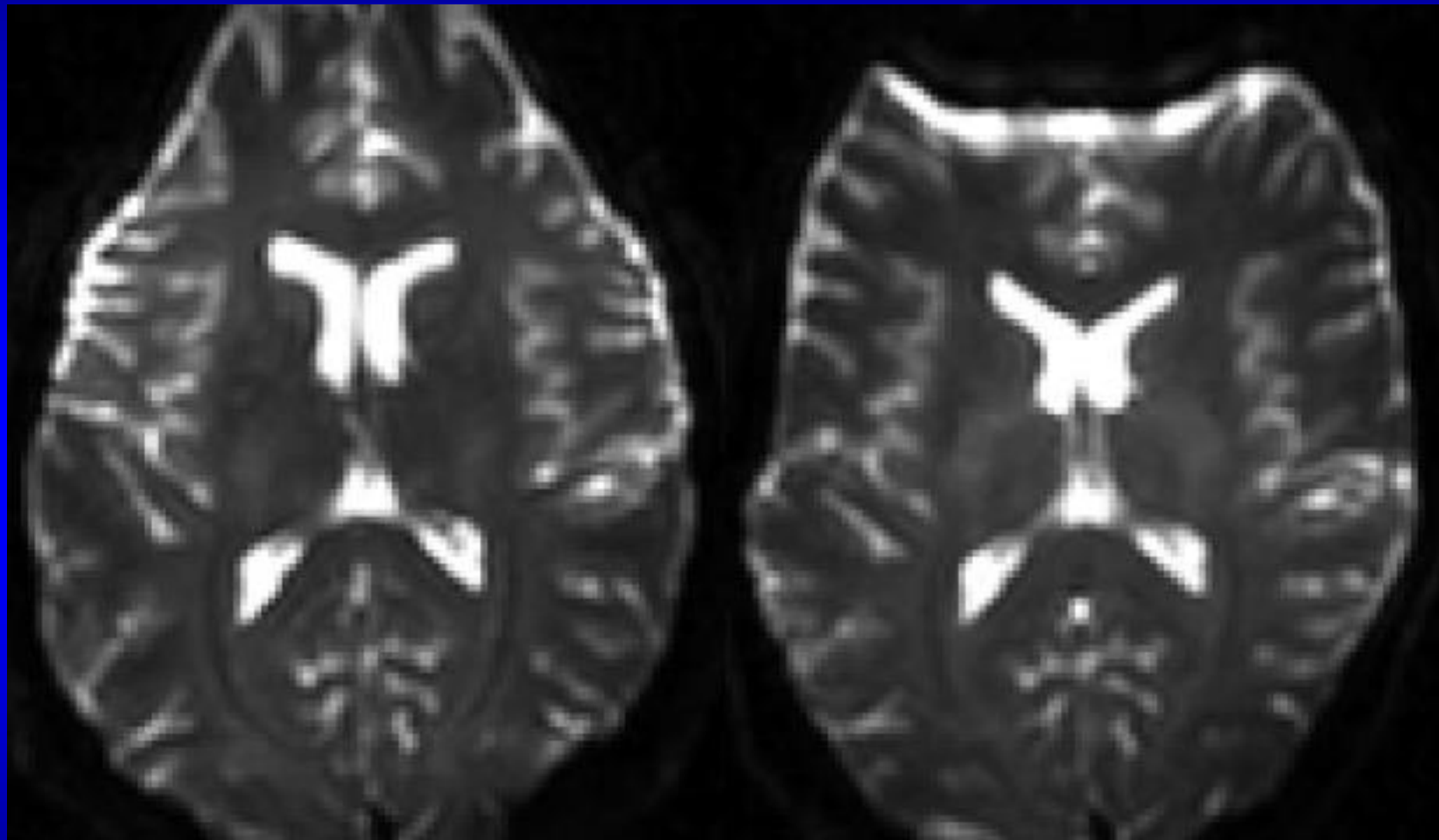
Published 3 September 2012

Online at stacks.iop.org/PMB/57/5715

EPI susceptibility artifact: An example

\mathcal{I}_1

\mathcal{I}_2



Outline

- **Introduction**
- **Method**
- **Results**
- **Discussion**

Outline

- **Introduction**
- **Method**
- **Results**
- **Discussion**

Introduction: Reason for field distortions

- **Fast (whole brain images in seconds) acquisition scheme of echo-planar imaging (EPI) is most frequently used for diffusion-weighted imaging (DWI) and diffusion-tensor imaging (DTI) (Stehling et al., 1991)**
- **Low acquisition bandwidth in phase encoding gradient direction (v) causes high sensitivity against small perturbations of the magnetic field (Chang & Fitzpatrick, 1992)**
- **Field inhomogeneities are caused by susceptibility differences and they scale with the B_0 field strength (Jezzard & Clare, 1999)**

Introduction: Correction approaches

- Field map approaches (Jezzard & Balaban, 1995) **suffer from long acquisition time and subject motion as well as regularization to overcome problems near tissue edges and regions with large inhomogeneities** (Holland et al., 2010)
- Point Spread Function **strategy** (Robson et al., 1997) **also takes several minutes for a full brain** (Holland et al., 2010)
- Direct registration **of EPI to anatomical images** (Merhof et al., 2007; Tao et al., 2009)
- Reversed gradient approach (Chang & Fitzpatrick, 1992; Morgan et al., 2004)

Our contribution: Reversed gradient approach with diffeomorphic transformation and thus meaningful intensity modulations (Ruthotto et al., 2012)

Outline

- **Introduction**
- **Method**
- **Results**
- **Discussion**

Method

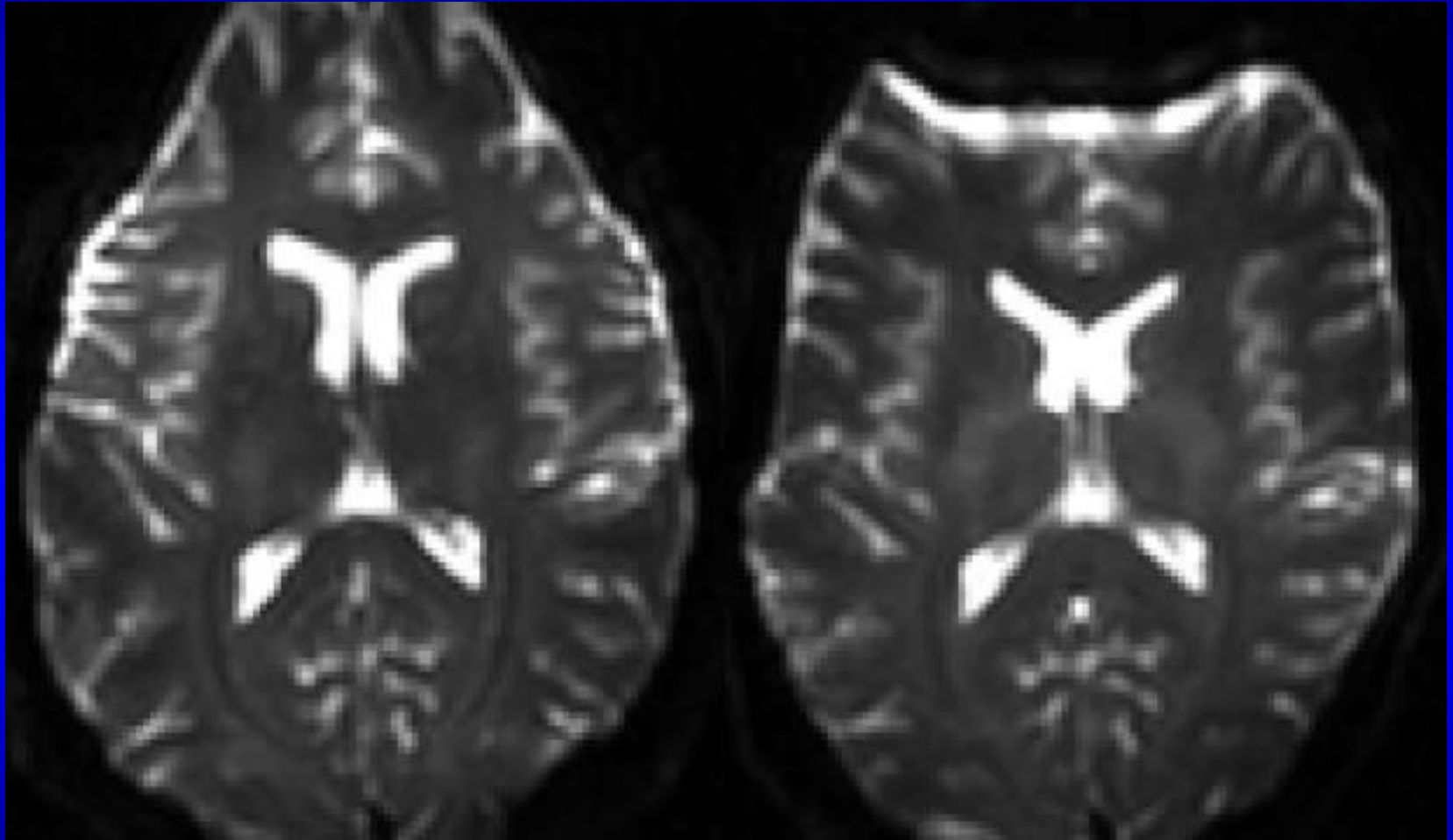
- Assuming a known field inhomogeneity $B : \Omega \rightarrow \mathbb{R}$ and the known direction of spatial mismatch $\mathbf{v} \in \mathbb{R}^3$, a forward model that relates the unobservable undistorted image $\mathcal{I} : \Omega \rightarrow \mathbb{R}$ to the observation $\mathcal{I}_1 : \Omega \rightarrow \mathbb{R}$ was introduced by (Chang & Fitzpatrick, 1992):

$$\mathcal{I}(\mathbf{x}) = \mathcal{I}_1(\mathbf{x} + B(\mathbf{x})\mathbf{v}) \cdot (1 + \partial_{\mathbf{v}}B) \quad \forall \mathbf{x} \in \Omega$$

- Requirement (Chang & Fitzpatrick, 1992): Measurement parameters have to be chosen such that the intensity modulation remains positive, corresponding to the invertibility of the mapping:

$$(1 + \partial_{\mathbf{v}}B(\mathbf{x})) \in]0, \infty[$$

Method

 \mathcal{I}_1 \mathcal{I}_2 

$$\mathcal{I}(\mathbf{x}) = \mathcal{I}_1(\mathbf{x} + B(\mathbf{x})\mathbf{v}) \cdot (1 + \partial_{\mathbf{v}}B) = \mathcal{I}_2(\mathbf{x} - B(\mathbf{x})\mathbf{v}) \cdot (1 - \partial_{\mathbf{v}}B) \quad \forall \mathbf{x} \in \Omega$$

Method: Functional to be minimized

$$\min_B \mathcal{J}(B) := \mathcal{D}(\mathcal{I}_1, \mathcal{I}_2; B)$$

$$\mathcal{D}(B) = \frac{1}{2} \int_{\Omega} (\mathcal{I}_1(\mathbf{x} + B(\mathbf{x})\mathbf{v}) \cdot (1 + \partial_{\mathbf{v}}B) - \mathcal{I}_2(\mathbf{x} - B(\mathbf{x})\mathbf{v})(1 - \partial_{\mathbf{v}}B))^2 d\mathbf{x}$$

$$\min_B \mathcal{J}(B) := \mathcal{D}(\mathcal{I}_1, \mathcal{I}_2; B) + \alpha \mathcal{S}^{\text{diff}}(B)$$

$$\mathcal{S}^{\text{diff}}(B) = \frac{1}{2} \int_{\Omega} |\nabla B(\mathbf{x})|^2 d\mathbf{x}$$

(Holland et al., 2010)

(Ruthotto et al., 2012)

$$\min_B \mathcal{J}(B) := \mathcal{D}(\mathcal{I}_1, \mathcal{I}_2; B) + \alpha \mathcal{S}^{\text{diff}}(B) + \beta \mathcal{S}^{\text{jac}}(B)$$

Method: Functional to be minimized

$$\min_B \mathcal{J}(B) := \mathcal{D}(\mathcal{I}_1, \mathcal{I}_2; B) + \alpha \mathcal{S}^{\text{diff}}(B) + \beta \mathcal{S}^{\text{jac}}(B)$$

$$\mathcal{D}(B) = \frac{1}{2} \int_{\Omega} (\mathcal{I}_1(\mathbf{x} + B(\mathbf{x})\mathbf{v}) \cdot (1 + \partial_{\mathbf{v}}B) - \mathcal{I}_2(x - B(\mathbf{x})\mathbf{v})(1 - \partial_{\mathbf{v}}B))^2 d\mathbf{x}$$

$$\mathcal{S}^{\text{diff}}(B) = \frac{1}{2} \int_{\Omega} |\nabla B(\mathbf{x})|^2 d\mathbf{x}$$

$$(1 + \partial_{\mathbf{v}}B(\mathbf{x})) \in]0, \infty[\text{ and } (1 - \partial_{\mathbf{v}}B(\mathbf{x})) \in]0, \infty[$$

which is equivalent to

$$\partial_{\mathbf{v}}B(\mathbf{x}) \in]-1, 1[$$

Method: Functional to be minimized

$$\min_B \mathcal{J}(B) := \mathcal{D}(\mathcal{I}_1, \mathcal{I}_2; B) + \alpha \mathcal{S}^{\text{diff}}(B) + \beta \mathcal{S}^{\text{jac}}(B)$$

$$\mathcal{S}^{\text{jac}}(B) = \int_{\Omega} \phi(\partial_{\mathbf{v}} B(\mathbf{x})) \, d\mathbf{x}, \quad \text{with } \phi(z) = \frac{z^4}{1 - z^2}$$

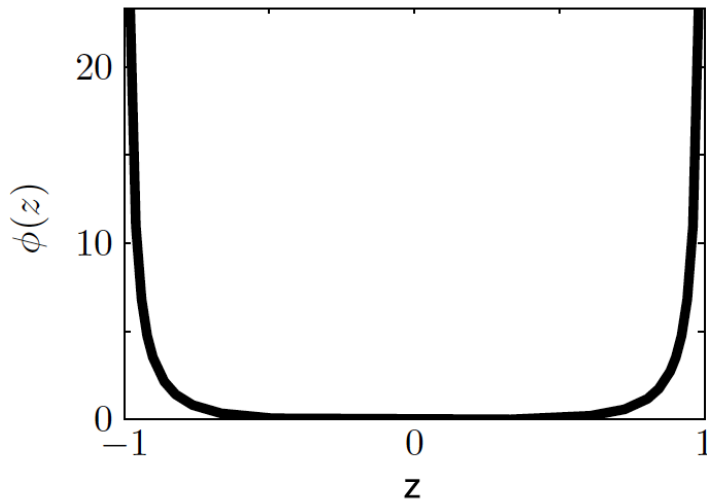


Figure 1. Plot of the proposed penalty function $\phi(z)$ acting on $\partial_{\mathbf{v}} B(\mathbf{x})$, see (7). The growth behavior of $\phi(z)$ to infinity as $|z| \rightarrow 1$ is crucial to ensure that the intensity modulations are positive almost everywhere and thus (5) is fulfilled. Since $1 \pm \partial_{\mathbf{v}} B(\mathbf{x})$ is the Jacobian determinant of the mapping $\mathbf{x} \pm B(\mathbf{x})\mathbf{v}$, this condition is equivalent to the diffeomorphy of the geometric transformation.

Method: Implementation and discretization

- **Follow guidelines of (Modersitzki, 2009)**
- **our model is implemented in SPM (google for SPM HYSCO) and as an extension to the freely available FAIR toolbox in Matlab (Modersitzki, 2009)**
- **Use a discretize-then-optimize approach on a hierarchy of levels to improve stability against local minima and give speed (Modersitzki, 2009)**
- **For computationally expensive routines such as image interpolation and regularization, parallelized C-code in a matrix free fashion is used (Modersitzki, 2009)**
- **Memory consumption is kept to a minimum and method runs on standard computer**

Method: MR measurements

- DT-MRI measured using Stejskal-Tanner spin-echo EPI
- Voxels of 1.875mm x 1.875mm x 3.6mm
- Contrast parameters: TR=9473, TE=95ms
- 20 direct. images, equally distrib. on sphere (Jones, 2004)
- Bandwidth in phase-encoding direction - selected as anterior-posterior- was 9.1 Hz pixel⁻¹, in frequency-encoding direction, it was 1675 Hz pixel⁻¹
- With one exception (difference 14%), the difference of mass (i.e. integral over I_1-I_2) was less than 1.5%
- Also only the image pair with “flat” diffusion gradient ($b=0$ s mm⁻²) is required for our correction, we acquired two full data sets with reversed gradients to investigate the impact of correction on Fractional Anisotropy (FA)

Definition of Fractional Anisotropy (FA)

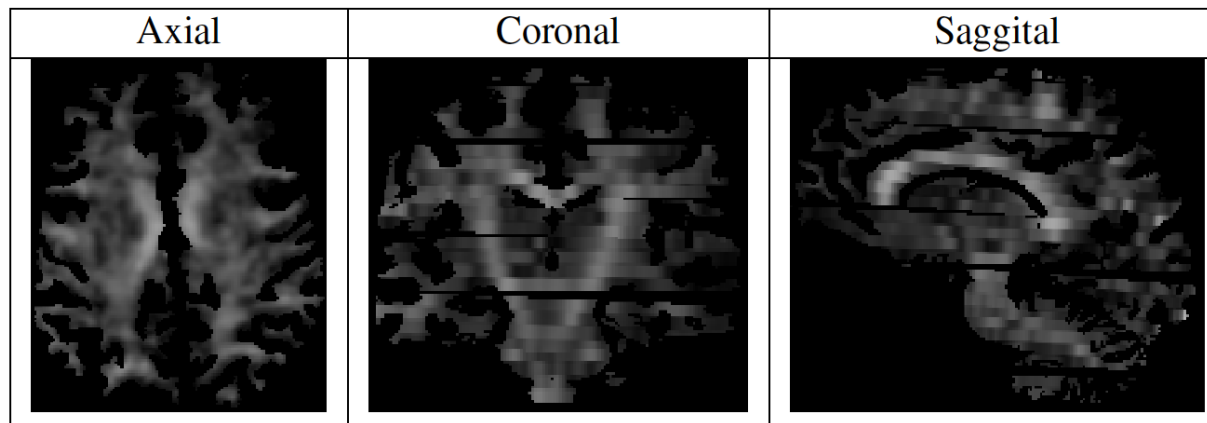


Figure 5.6: *Fractional anisotropy index, FA (see Equation (5.16)), of the DT-MRI, masked with the WM mask.*

When extracting the anisotropic part of the matrix of the diffusion tensor, $\mathbf{A} \in \mathbb{R}^{3 \times 3}$, by means of

$$\mathbf{A} := \mathbf{D} - \frac{\text{trace} \mathbf{D}}{3} \mathbf{Id}, \quad (5.15)$$

the *fractional anisotropy index* FA is defined as [21]

$$\text{FA} := \sqrt{\frac{3}{2} \frac{\sqrt{\mathbf{A} : \mathbf{A}}}{\sqrt{\mathbf{D} : \mathbf{D}}}} \quad \text{with} \quad \mathbf{B} : \mathbf{C} \equiv \sum_{i,j=1}^3 B^{[ij]} C^{[ij]}. \quad (5.16)$$

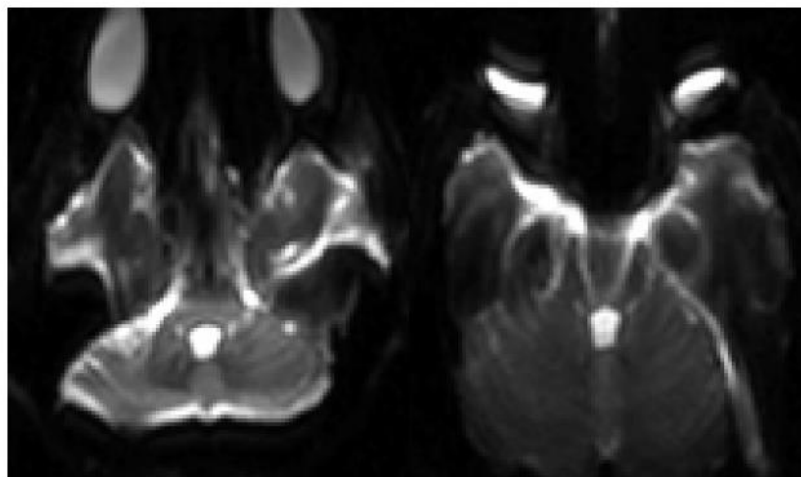
Figure 5.6 shows a map of the fractional anisotropy index of the registered DT data, masked with the WM mask. With $FA = 0.74$, the highest value for fractional anisotropy was found in the splenium of the corpus callosum. Note also the strong anisotropy of the pyramidal tract in the figure.

Outline

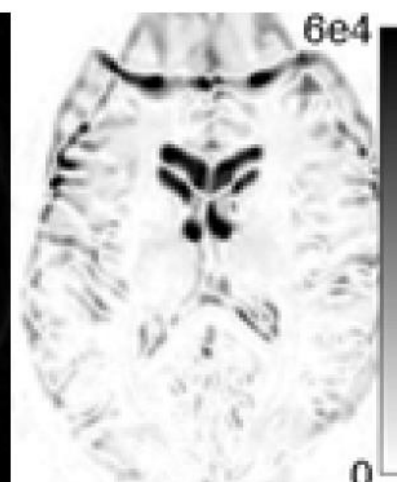
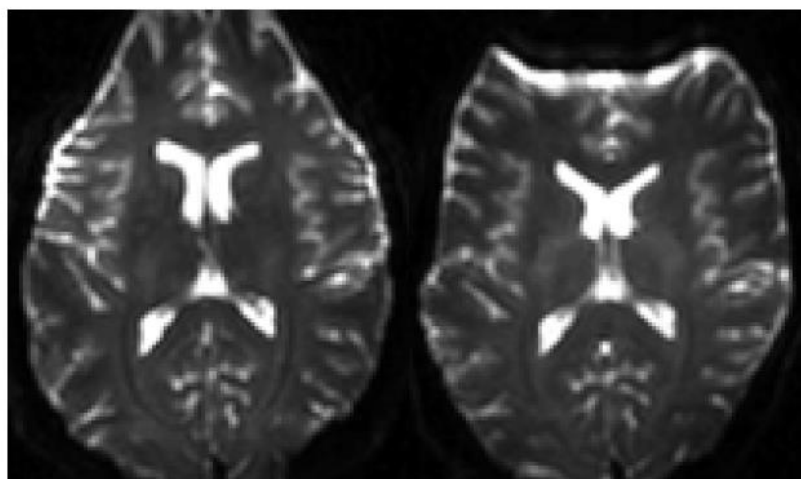
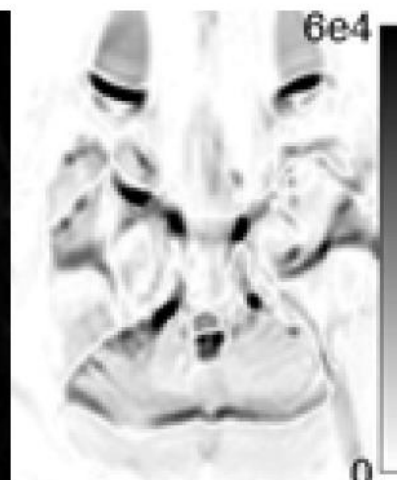
- **Introduction**
- **Method**
- **Results**
- **Discussion**

Results

initial data



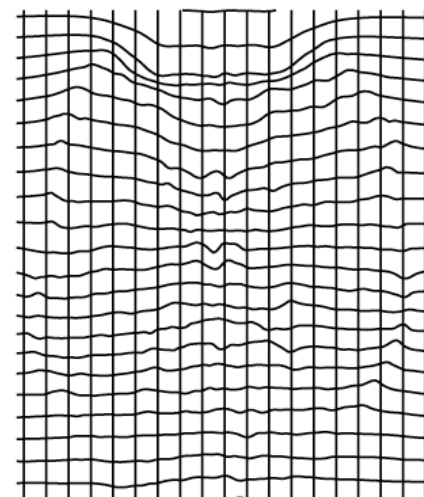
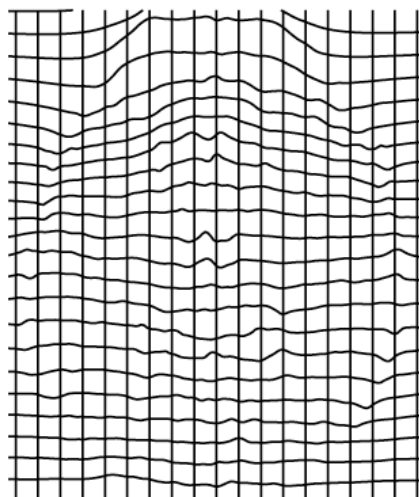
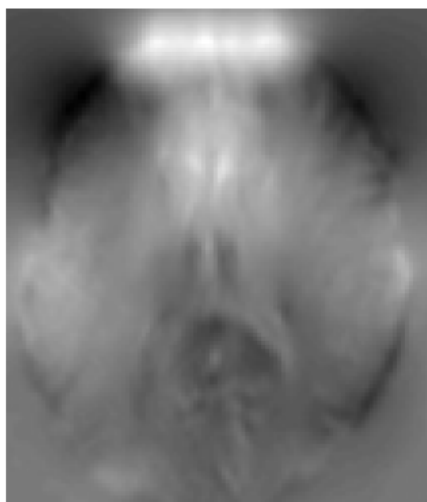
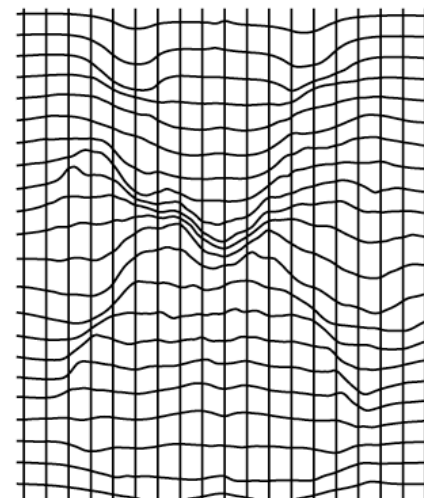
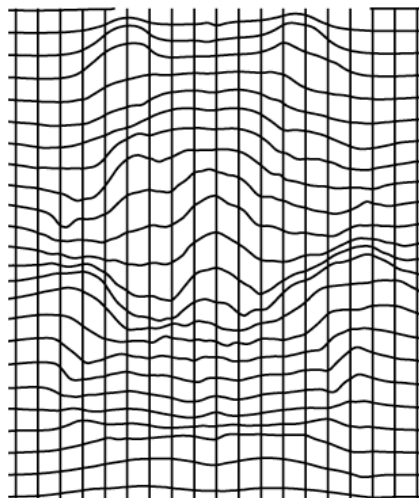
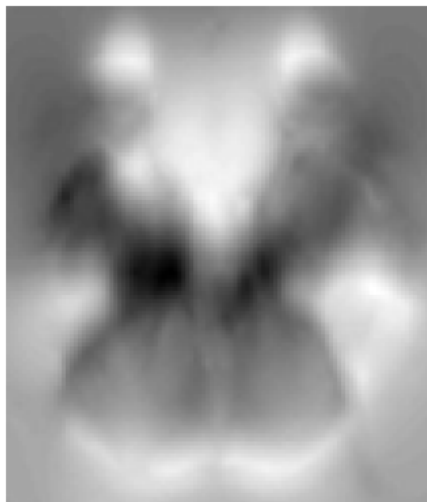
difference



Results

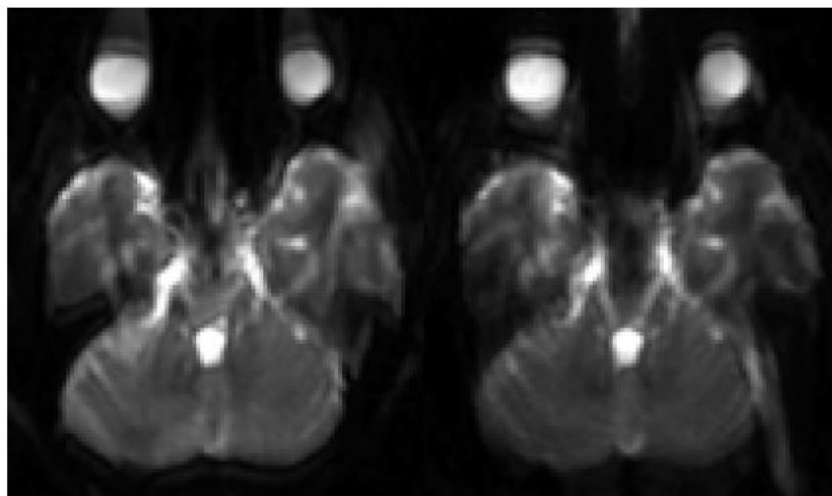
estimated B

transformations

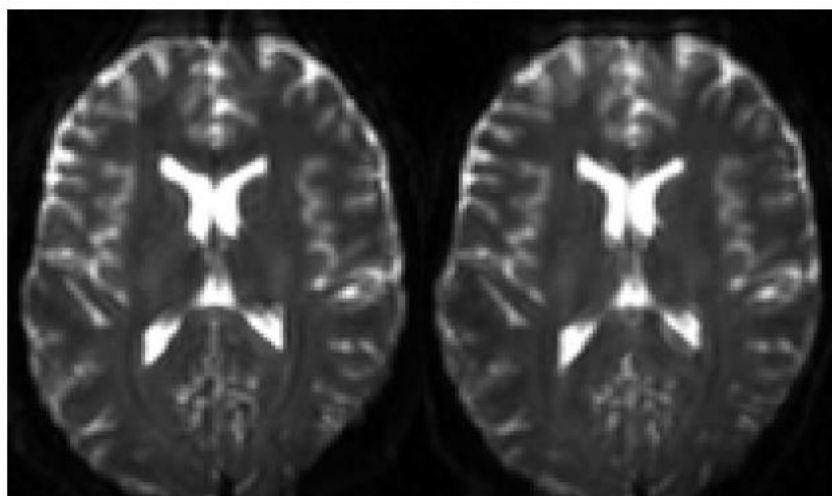
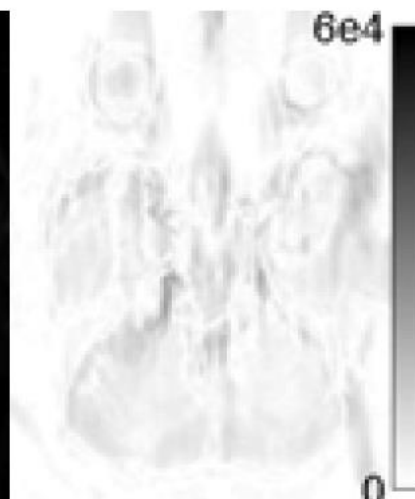


Results

corrected data



difference

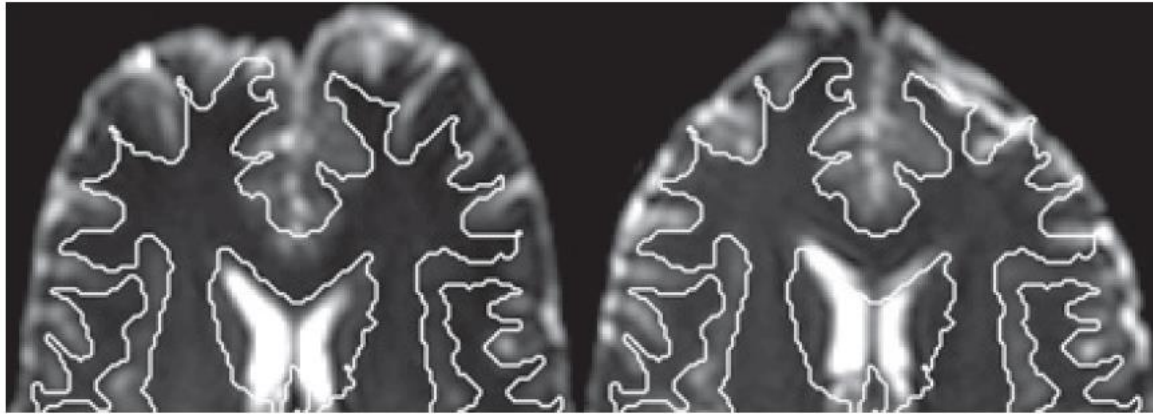


Results

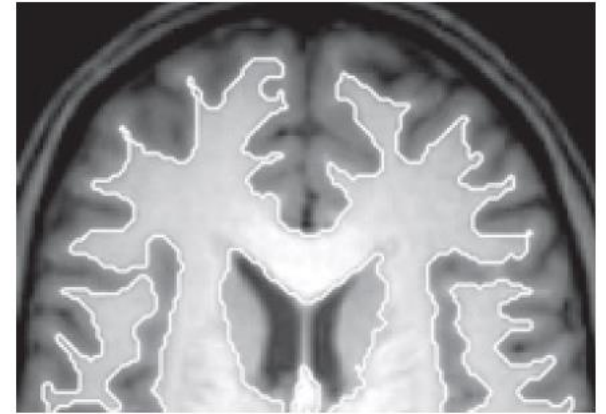
Table 1. Results of susceptibility correction for the six DTI datasets: reduction in the distance measure \mathcal{D} (second column), normalized cross-correlation between \mathcal{I}_1 and \mathcal{I}_2 before ($\mathcal{NCC}(0)$, third column) and after ($\mathcal{NCC}(B)$, fourth column) registration. The range $\partial_v B$ (fifth column) is a measure of registration regularity and the range of B (sixth column) is a measure of the maximal deformation. Runtime (seventh column) and number of iterations on the different levels (from coarse to fine) of the multi-level optimization approach (eighth column).

Dataset	$\frac{\mathcal{D}(B)}{\mathcal{D}(0)}$	$\mathcal{NCC}(0)$	$\mathcal{NCC}(B)$	Range $\partial_v B$	Range(B)	Runtime (s)	Iterations
DTI-1	0.04	0.74	0.98	$[-0.92, 0.86]$	$[-18.5, 30.3]$	133	[10, 4, 4, 6]
DTI-2	0.04	0.74	0.98	$[-0.91, 0.89]$	$[-16.0, 28.8]$	100	[10, 5, 3, 3]
DTI-3	0.05	0.66	0.97	$[-0.89, 0.91]$	$[-24.1, 29.1]$	80	[10, 6, 4, 2]
DTI-4	0.05	0.69	0.97	$[-0.90, 0.84]$	$[-19.7, 24.1]$	70	[10, 4, 3, 2]
DTI-5	0.05	0.72	0.98	$[-0.91, 0.90]$	$[-14.1, 30.6]$	87	[10, 3, 3, 3]
DTI-6	0.04	0.72	0.98	$[-0.91, 0.89]$	$[-16.3, 22.8]$	63	[10, 4, 3, 2]

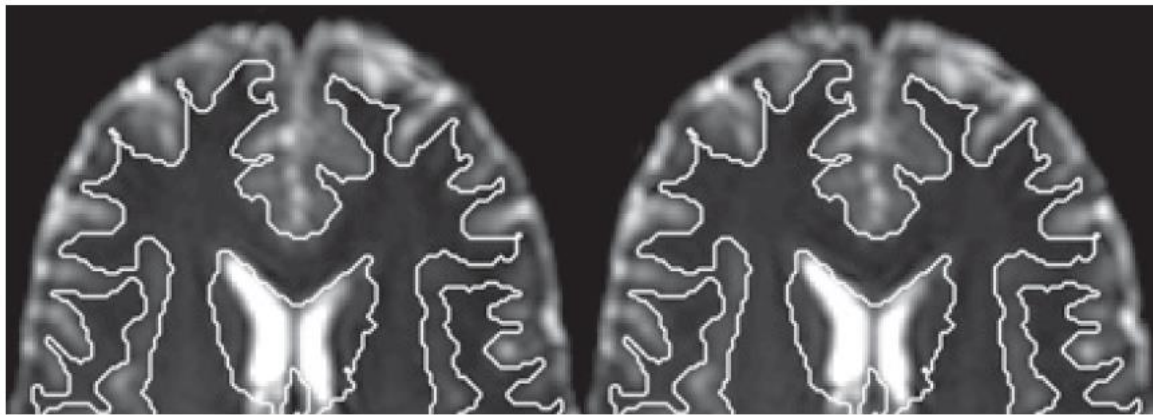
Results



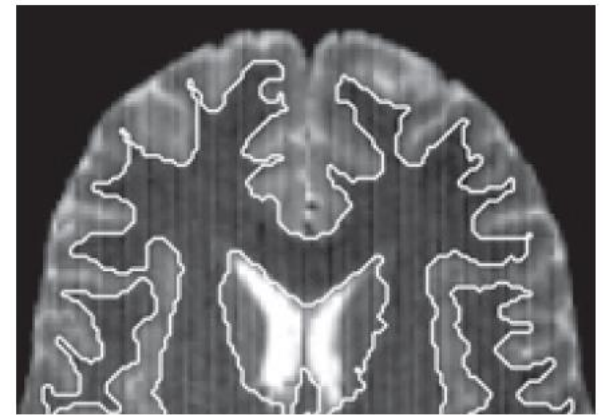
(a) initial data ($b = 0$)



(b) T1 weighted MRI

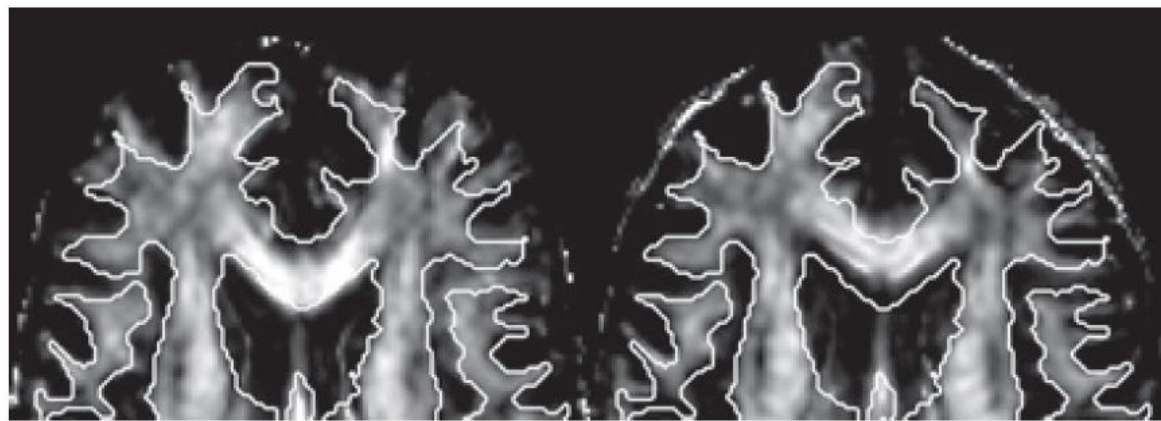


(c) corrected data ($b = 0$)

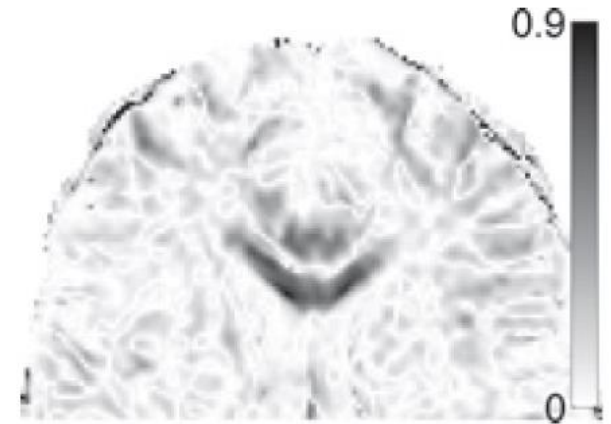


(d) T2 weighted MRI

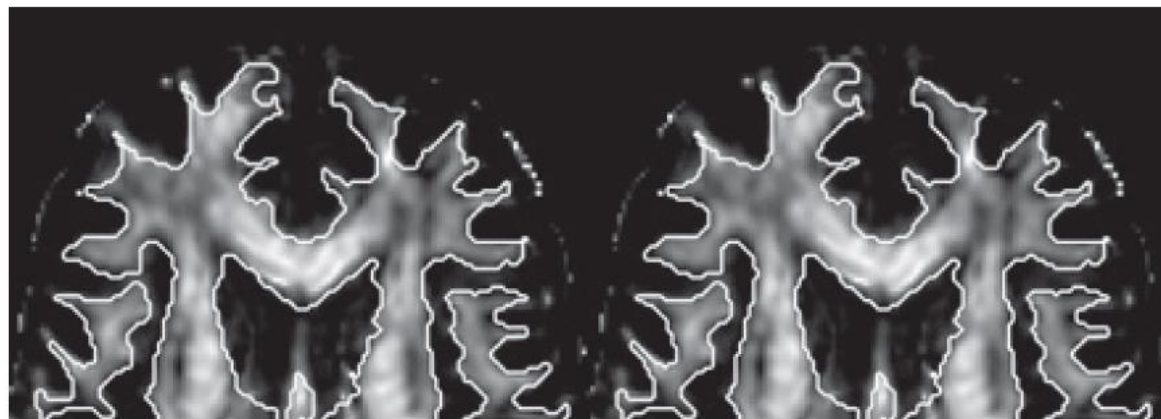
Results: Fractional Anisotropy (FA)



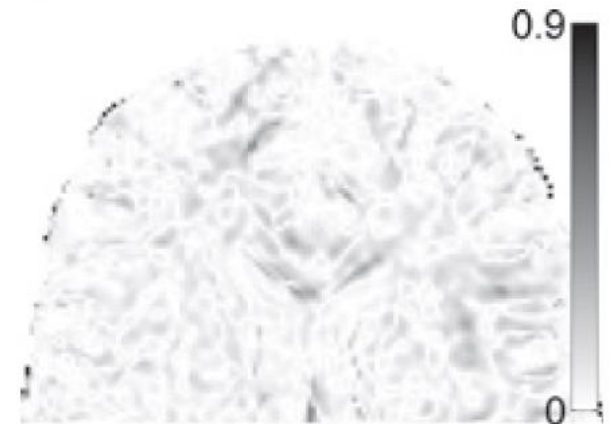
(e) FA map uncorrected data



(f) FA difference = 100 %



(g) FA map after correction



(h) FA difference = 63 %

Results

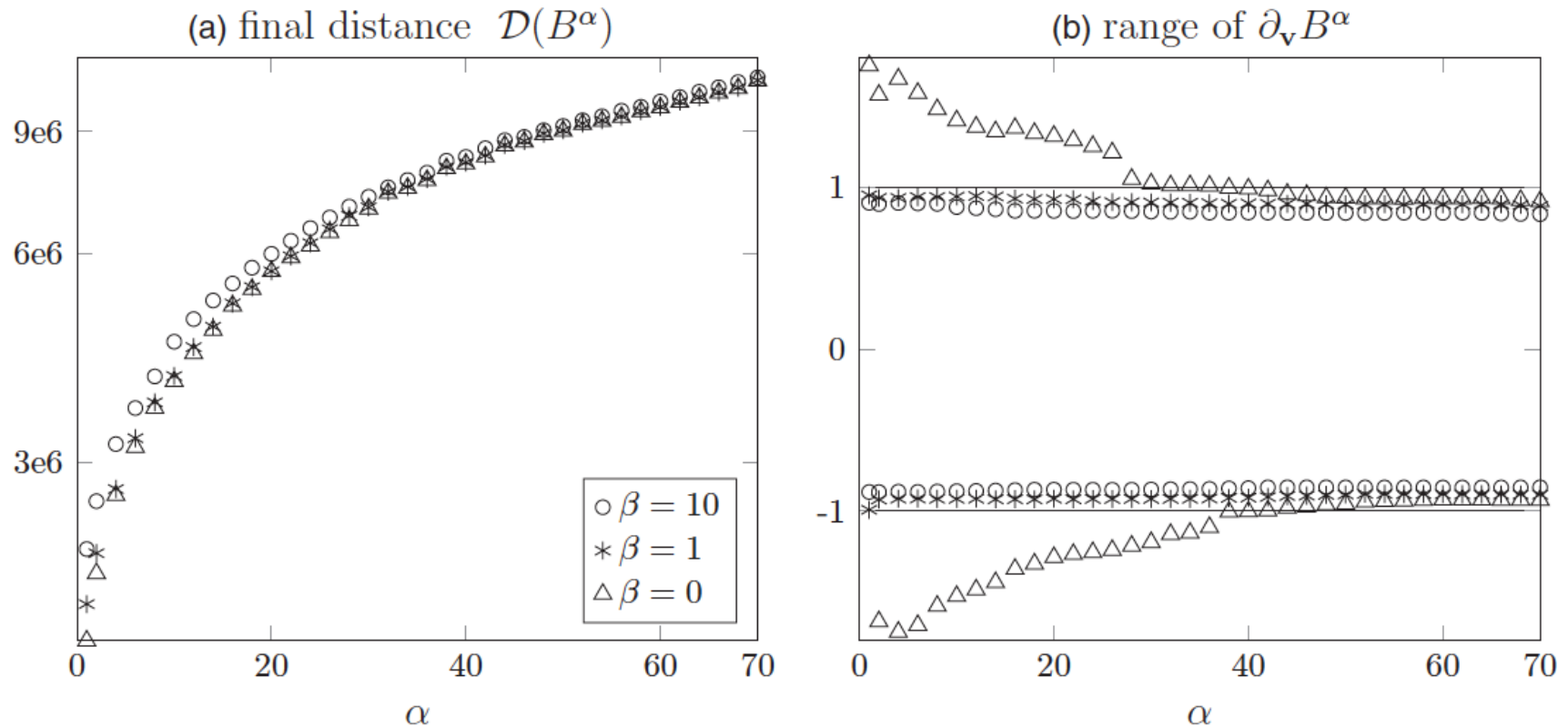


Figure 4. Comparison of diffusion regularization scheme (Δ , $\beta = 0$) as in Holland *et al* (2010) with the proposed extension by the nonlinear regularization term \mathcal{S}^{jac} in (7) ($*$, $\beta = 1$; \circ , $\beta = 10$). The final image distances, depicted in a semi-logarithmic plot (a) for α increasing from 1 to 70, are at a comparable level for all tested choices of β . As to be expected, the image distance is reduced marginally more for $\beta = 0$. However, in plot (b), visualizing the range of $\partial_{\mathbf{v}} B^\alpha$, it can be seen that the regularity condition (6) is violated for $\beta = 0$ and small values of α . For $\beta = 1, 10$, the range is in the interval $[-0.99, 0.84]$ for all tested α .

Outline

- **Introduction**
- **Theory**
- **Results**
- **Discussion**

Discussion

- **Necessary additional amount of measurement time: <1min**
- **Compared to (Holland et al., 2010), a key novelty of our reversed gradient approach is the additional nonlinear regularizer that guarantees positive intensity modulations and diffeomorphic geometrical transformations independent of the actual choice of regularization parameters**
- **Not very sensitive to choice of regularization parameters, our choice was fine for all 6 of our investigated DTI datasets**
- **Effective reduction of distortions and further reduction possible when combining our approach with parallel imaging**
- **When compared to (Chang & Fitzpatrick, 1992; Morgan et al., 2004; Weiskopf et al., 2005), our approach doesn't need any pre-segmentation and edge detection**

Discussion

- **When compared to (Andersson et al., 2003; Skare & Andersson, 2005), computational expenses were lowered due to non-parametric transformation, high-end optimization and multi-level techniques**
- **Approach is not limited to EPI, as the underlying physical distortion model was first developed for any inhomogeneity-induced artifacts in MR (Chang & Fitzpatrick, 1992)**
- **The assumption of no signal loss (mass-preservation) is well satisfied by spin-echo, but it is only approximately fulfilled by gradient echo schemes commonly used in fMRI, but first fMRI results suggest that our method is also valuable for fMRI**

Thank you for your attention

